

Accepted Manuscript

Analysis of cracked functionally graded piezoelectric strip

S.M. Mousavi, J. Paavola

PII: S0020-7683(13)00147-9

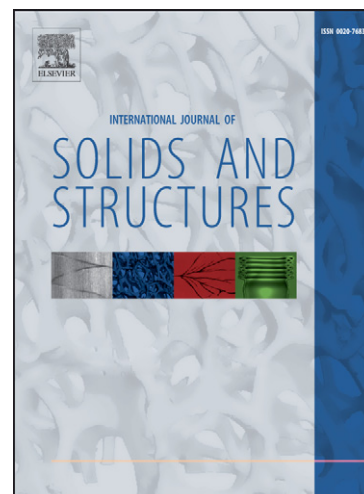
DOI: <http://dx.doi.org/10.1016/j.ijsolstr.2013.03.038>

Reference: SAS 7959

To appear in: *International Journal of Solids and Structures*

Received Date: 9 October 2012

Revised Date: 20 March 2013



Please cite this article as: Mousavi, S.M., Paavola, J., Analysis of cracked functionally graded piezoelectric strip, *International Journal of Solids and Structures* (2013), doi: <http://dx.doi.org/10.1016/j.ijsolstr.2013.03.038>

This is a PDF file of an unedited manuscript that has been accepted for publication. As a service to our customers we are providing this early version of the manuscript. The manuscript will undergo copyediting, typesetting, and review of the resulting proof before it is published in its final form. Please note that during the production process errors may be discovered which could affect the content, and all legal disclaimers that apply to the journal pertain.

Analysis of cracked functionally graded piezoelectric strip

S. M. Mousavi^{1,*}, J. Paavola¹

¹*Department of Civil and Structural Engineering, Rakentajanaukio 4 A, Otaniemi, FI-02150 Espoo Finland*

^{*}*Corresponding author-Email Address: mahmoud.mousavi@aalto.fi*

Tel: +358503503184

Abstract

The fracture behavior of a cracked strip under antiplane mechanical and inplane electrical loading is studied. A functionally graded piezoelectric strip with exponential material gradation is under consideration. The mechanical and electrical loading is combined via loading coupling factor. The problem of a graded piezoelectric strip containing a screw dislocation is solved. This solution results in stress and electric displacement components with Cauchy singularity. Based on the solution achieved for the dislocation, the distributed dislocation technique (DDT) is utilized to form any geometry of multiple cracks and analyze the behavior of a cracked strip under antiplane mechanical and inplane electrical loading. This technique is capable of the analysis of a strip with a system of interacting cracks. Several examples including strips with single crack, two straight cracks and two curved cracks are presented.

Keywords

Functionally graded piezoelectric; Crack; Strip; Distributed Dislocation Technique.

1. Introduction

Piezoelectric materials have been utilized in some advanced applications which necessitate the analysis of their behavior in different situations. Due to the behavior of piezoelectric materials, they are usually susceptible to crack. Therefore, these materials have been the subject of many researches in the field of fracture mechanics. Different loadings can be recognized in various applications of piezoelectric materials including static (Chen et al., 2003), time-harmonic (Ma et al., 2004, 2005a; Narita and Shindo, 1999) and transient (Chen et al., 2004) types.

The piezoelectric materials may be homogeneous or nonhomogeneous. The most common assumption for material gradation is exponential dependence to the location (Chen and Liu, 2005).

The crack boundary conditions may be assumed permeable (Parton and Mikhailov, 1990), impermeable (Sosa, 1992) or partially permeable. The experimental investigations depict that the electric loading has dominant effect on the fracture behavior of the piezoelectric materials which is coincident with the impermeability condition (Wang and Yu, 2000).

On the other hand, various arrangements of defects may exist in a structure. Many useful published articles are devoted to specific crack geometries in the strip. However, the capability to characterize the behavior of the cracked strip in the presence of multi arbitrary cracks still needs more investigations.

Distributed Dislocation Technique (DDT) provides the capability to tackle various configurations of cracks. In this technique, the initial and fundamental step is to analyze the domain in the presence of a dislocation. Subsequently by utilizing the dislocation solution, superposition and the Buckner's principle (Korsunsky and Hills, 1996), it is possible to form any geometry of the cracks and achieve the strip's behavior and field intensity factors. DDT has been utilized for static and recently for elastodynamic analyses of cracked domain under mechanical loading. Wang et al. have studied interacting dielectric cracks in piezoelectric

materials utilizing DDT (Wang and Jiang, 2002). This technique has also been proved to be useful in the analysis of axisymmetric annular cracks in a piezoelectric medium under static loading (Asadi, 2011). DDT has been utilized to calculate the plane electro-elastic fields in piezoelectric materials with multiple cracks (Han and Wang, 1999). The effect of viscous damping in functionally graded material (FGM) has been also analyzed via DDT (Mousavi and Fariborz, 2012). A detailed study about the Fracture mechanics of piezoelectric materials is carried out by Kuna (2010).

In the present article, the dislocation solution is achieved for a strip under antiplane mechanical and inplane electrical loading. The electrically impermeable crack face assumption is used as the dislocation condition. Afterward, the distributed dislocation technique is utilized for the antiplane analysis of a cracked functionally graded piezoelectric (FGP) strip. The stress and electric intensity factors are determined for cracked strip. The configuration and arrangement of cracks in the strip is arbitrary and some samples are presented.

2. Solution of functionally graded piezoelectric strip containing screw dislocation

Consider the Functionally Graded Piezoelectric (FGP) strip wherein material properties gradations take place in the thickness direction. The poling direction is also assumed in the same direction. A Volterra-type screw dislocation with the line of dislocation parallel to x -axis is located in the strip at a point with coordinates (η, ζ) , Fig. 1.

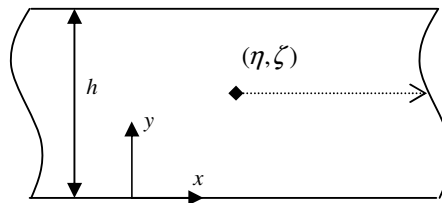


Fig. 1. Schematic view of the FGP strip weakened by a screw dislocation

The plane of analysis is chosen to be the x - y plane. Therefore the inplane electric fields couple only with the antiplane elastic fields which is called antiplane strain problem. The displacement field components, including $[u, v, w]$, and the electric field components, including $[E_x, E_y, E_z]$ in the electroelastic boundary value problem for antiplane displacement and inplane electric fields are (Narita and Shindo 1999; Pak and Goloubeva, 1996).

$$\begin{aligned} u &\equiv 0, \quad v \equiv 0, \quad w \equiv w(x, y) \\ E_x &= E_x(x, y), \quad E_y = E_y(x, y), \quad E_z \equiv 0 \end{aligned} \quad (1)$$

The electric fields $[E_x, E_y]$ are related to the electrical potential $\phi(x, y)$ as

$$E_x = -\frac{\partial \phi}{\partial x}, \quad E_y = -\frac{\partial \phi}{\partial y} \quad (2)$$

In FGP material, the constitutive equations for inplane electric fields coupling with the antiplane elastic fields are (Chen et al., 2003)

$$\begin{aligned} \sigma_{xz} &= c_{44}(y) \frac{\partial w}{\partial x} + e_{15}(y) \frac{\partial \phi}{\partial x} \\ \sigma_{yz} &= c_{44}(y) \frac{\partial w}{\partial y} + e_{15}(y) \frac{\partial \phi}{\partial y} \\ D_x &= e_{15}(y) \frac{\partial w}{\partial x} - d_{11}(y) \frac{\partial \phi}{\partial x} \\ D_y &= e_{15}(y) \frac{\partial w}{\partial y} - d_{11}(y) \frac{\partial \phi}{\partial y} \end{aligned} \quad (3)$$

in which $c_{44}(y)$, $e_{15}(y)$ and $d_{11}(y)$ are the shear modulus measured in a constant electric field, the piezoelectric constant and dielectric constant measured at a constant strain, respectively.

Also $\sigma_{xz}(x, y)$ and $\sigma_{yz}(x, y)$ are the shear stress components while $D_x(x, y)$ and $D_y(x, y)$ are the electric displacement components. In the absence of body forces and charges, the mechanical equilibrium equation for the stress components and the electric Maxwell equation for the electric displacement components are

$$\begin{aligned}\frac{\partial \sigma_{xz}}{\partial x} + \frac{\partial \sigma_{yz}}{\partial y} &= 0 \\ \frac{\partial D_x}{\partial x} + \frac{\partial D_y}{\partial y} &= 0\end{aligned}\tag{4}$$

Substituting equations (3) into equations (4) yields

$$\begin{aligned}c_{44}(y)\Delta w + e_{15}(y)\Delta\phi + \frac{\partial c_{44}(y)}{\partial y}\frac{\partial w}{\partial y} + \frac{\partial e_{15}(y)}{\partial y}\frac{\partial \phi}{\partial y} &= 0 \\ e_{15}(y)\Delta w - d_{11}(y)\Delta\phi + \frac{\partial e_{15}(y)}{\partial y}\frac{\partial w}{\partial y} - \frac{\partial d_{11}(y)}{\partial y}\frac{\partial \phi}{\partial y} &= 0\end{aligned}\tag{5}$$

in which Δ is the two dimensional Laplacian operator. The properties of FGP material are assumed to be varying in y -direction and described in terms of exponential functions along the strip thickness. In order to overcome the complexity of the mathematics involved, the focus is limited on a special class of FGP materials in which the variations of these properties obey the same exponential law (Chen et al., 2003; Ma et al., 2004).

$$[c_{44}(y), e_{15}(y), d_{11}(y)] = [c_{44}^0, e_{15}^0, d_{11}^0] \exp(2\kappa y)\tag{6}$$

while c_{44}^0 , e_{15}^0 and d_{11}^0 are constants. The assumption in (6) is one of the cases which make the boundary value problem (equations 5) analytically treatable and is generally applied for FGP materials (Erdogan and Ozturk, 1992). Therefore, this specific case will allow us to shed some light on the influence of the material gradient upon the stress and electric intensity factors. Applying equations (6) into equations (5) results in

$$\begin{aligned}c_{44}^0\Delta w + e_{15}^0\Delta\phi + 2\kappa c_{44}^0\frac{\partial w}{\partial y} + 2\kappa e_{15}^0\frac{\partial \phi}{\partial y} &= 0 \\ e_{15}^0\Delta w - d_{11}^0\Delta\phi + 2\kappa e_{15}^0\frac{\partial w}{\partial y} - 2\kappa d_{11}^0\frac{\partial \phi}{\partial y} &= 0\end{aligned}\tag{7}$$

Utilizing the Bleustein function, (Bleustein, 1968)

$$\psi(x, y) = \phi - \alpha w \quad (8)$$

in which $\alpha = \frac{e_{15}^0}{d_{11}^0}$, equations (7) are decoupled to the following form

$$\begin{aligned} \Delta w + 2\kappa \frac{\partial w}{\partial y} &= 0 \\ \Delta \psi + 2\kappa \frac{\partial \psi}{\partial y} &= 0 \end{aligned} \quad (9)$$

In terms of variables w and ψ , the constitutive equations (3) can be written as follows

$$\begin{aligned} \sigma_{xz} &= [c_{44}(y) + \alpha e_{15}(y)] \frac{\partial w}{\partial x} + e_{15}(y) \frac{\partial \psi}{\partial x} \\ \sigma_{yz} &= [c_{44}(y) + \alpha e_{15}(y)] \frac{\partial w}{\partial y} + e_{15}(y) \frac{\partial \psi}{\partial y} \\ D_x &= -d_{11}(y) \frac{\partial \psi}{\partial x} \\ D_y &= -d_{11}(y) \frac{\partial \psi}{\partial y} \end{aligned} \quad (10)$$

It has been found that impermeable crack assumption is more coincident with experimental results (Wang and Yu, 2000). Assuming impermeable condition for the strip weakened by a screw dislocation (Fig. 1), the boundary, continuity and limiting conditions will be expressed as

$$\begin{aligned} \sigma_{yz}(x, 0) &= 0, \quad \sigma_{yz}(x, h) = 0, \quad \sigma_{yz}(x, \zeta^-) = \sigma_{yz}(x, \zeta^+) \\ D_y(x, 0) &= 0, \quad D_y(x, h) = 0, \quad D_y(x, \zeta^-) = D_y(x, \zeta^+) \\ w(x, \zeta^-) - w(x, \zeta^+) &= b_{wz} H(x - \eta), \quad \lim_{|x| \rightarrow \infty} w = 0 \\ \phi(x, \zeta^-) - \phi(x, \zeta^+) &= b_{\phi z} H(x - \eta), \quad \lim_{|x| \rightarrow \infty} \phi = 0 \end{aligned} \quad (11)$$

while $b_{wz}, b_{\phi z}$ are the dislocation Burgers vectors and $H(..)$ is the Heaviside step-function.

Although the jump in the electric potential is not a type of dislocation, it is referred here as

the electric dislocation for convenience. In order to solve the equations (9), equation (8) is applied to the conditions (11)

$$\begin{aligned}\sigma_{yz}(x, 0) &= 0, \sigma_{yz}(x, h) = 0, \sigma_{yz}(x, \zeta^-) = \sigma_{yz}(x, \zeta^+) \\ D_y(x, 0) &= 0, D_y(x, h) = 0, D_y(x, \zeta^-) = D_y(x, \zeta^+) \\ w(x, \zeta^-) - w(x, \zeta^+) &= b_{wz} H(x - \eta) \\ \psi(x, \zeta^-) - \psi(x, \zeta^+) &= (b_{\phi z} - \alpha b_{wz}) H(x - \eta)\end{aligned}\tag{12}$$

and,

$$\begin{aligned}\lim_{|x| \rightarrow \infty} w &= 0 \\ \lim_{|x| \rightarrow \infty} \psi &= 0\end{aligned}$$

Equations (9) may be solved by means of the complex Fourier transform defined by

$$f^*(s) = \int_{-\infty}^{\infty} f(x) \exp(-isx) dx\tag{13}$$

The inversion of (13) is

$$f(x) = \frac{1}{2\pi} \int_{-\infty}^{\infty} f^*(s) \exp(isx) ds\tag{14}$$

With the aid of complex Fourier transforms and equations (8, 9, 10, 12), the functions w and

ϕ are determined.

$$\begin{aligned}w(x, y) &= \frac{b_{wz} \exp(\kappa \zeta)}{2} L(h - \zeta) - \frac{ib_{wz} \exp(-\kappa(y - \zeta))}{2\pi} P_1(y, h - \zeta) & 0 \leq y \leq \zeta \\ w(x, y) &= -\frac{b_{wz} \exp(-\kappa(h - \zeta))}{2} L(\zeta) + \frac{ib_{wz} \exp(-\kappa(y - \zeta))}{2\pi} P_1(y - h, \zeta) & \zeta \leq y \leq h \\ \phi(x, y) &= \frac{b_{\phi z} \exp(\kappa \zeta)}{2} L(h - \zeta) - \frac{ib_{\phi z} \exp(-\kappa(y - \zeta))}{2\pi} P_1(y, h - \zeta) & 0 \leq y \leq \zeta \\ \phi(x, y) &= -\frac{b_{\phi z} \exp(-\kappa(h - \zeta))}{2} L(\zeta) + \frac{ib_{\phi z} \exp(-\kappa(y - \zeta))}{2\pi} P_1(y - h, \zeta) & \zeta \leq y \leq h\end{aligned}\tag{15}$$

in which $\beta^2 = \kappa^2 + s^2$, $L(\gamma) = \sinh(\kappa\gamma)/\sinh(\kappa h)$ and $P_1(\gamma_1, \gamma_2)$ is given in Appendix A. This is the solution for a dislocation parallel with x -axis in Fig. 1. The same procedure may be carried out for a vertical dislocation. The results are coincident with horizontal dislocation which proves that the line of dislocation is arbitrary and does not affect the field equation of a dislocation in the domain.

Stress and electric displacement components can be determined utilizing equations (15) and the equations (6, 8, 10):

$$\begin{aligned} \begin{Bmatrix} \sigma_{xz} \\ D_x \end{Bmatrix} &= \begin{Bmatrix} \chi_1 \\ -\chi_2 \end{Bmatrix} P_2(y, h - \zeta) & 0 \leq y \leq \zeta \\ \begin{Bmatrix} \sigma_{xz} \\ D_x \end{Bmatrix} &= \begin{Bmatrix} -\chi_1 \\ \chi_2 \end{Bmatrix} P_2(y - h, \zeta) & \zeta \leq y \leq h \\ \begin{Bmatrix} \sigma_{yz} \\ D_y \end{Bmatrix} &= i \begin{Bmatrix} -\chi_1 \\ \chi_2 \end{Bmatrix} P_3(y, h - \zeta) & 0 \leq y \leq \zeta \\ \begin{Bmatrix} \sigma_{yz} \\ D_y \end{Bmatrix} &= i \begin{Bmatrix} \chi_1 \\ -\chi_2 \end{Bmatrix} P_3(y - h, \zeta) & \zeta \leq y \leq h \end{aligned} \quad (16)$$

in which $\chi_1 = (b_{wz} c_{44}^0 + b_{\square z} e_{15}^0) \exp(\kappa(y + \zeta)) / (2\pi)$, $\chi_2 = (b_{\square z} - a b_{wz}) d_{11}^0 \exp(\kappa(y + \zeta)) / (2\pi)$ and $P_2(\gamma_1, \gamma_2)$ and $P_3(\gamma_1, \gamma_2)$ are given in Appendix A.

2.1 Singularity analysis

The stress and electric displacement components for a dislocation are singular in the vicinity of the dislocation. This is verified with the aid of the following integral equations (Abramowitz and Stegun, 1964).

$$\begin{aligned} \int_0^\infty \exp(sy) \sin(sx) ds &= x / (x^2 + y^2), \quad y < 0 \\ \int_0^\infty \exp(sy) \cos(sx) ds &= -y / (x^2 + y^2), \quad y < 0 \end{aligned} \quad (17)$$

With the aid of the above integral equations, the singular terms in the Stress and electric displacement components in equations (16) may be separated. These forms of field components are given in Appendix B. As was expected, the above mentioned field components depict Cauchy singularity in the vicinity of the dislocation.

3. Crack formulation

The solution for the dislocation in the FGP strip can be utilized for the analysis of cracked strip via distributed dislocation technique (Fotuhi and Fariborz, 2006). Let the strip be weakened by N cracks including N_I embedded and $N-N_I$ edge cracks, described in parametric form as

$$\begin{aligned} x_k &= \alpha_k(s), \\ y_k &= \beta_k(s), \quad k \in \{1, 2, \dots, N\}, \quad -1 \leq s \leq 1. \end{aligned} \quad (18)$$

The moveable orthogonal coordinate system (n, t) is chosen such that the origin may move on the crack while t -axis remains tangent to the crack surface (Fig. 2). On the surface of the k th crack, the traction and electric displacement components in the Cartesian coordinates (x, y) become

$$\begin{aligned} \sigma_{nz}(x_k, y_k) &= \sigma_{yz} \cos(\theta_k) - \sigma_{xz} \sin(\theta_k) \\ D_n(x_k, y_k) &= D_y \cos(\theta_k) - D_x \sin(\theta_k) \quad k \in \{1, 2, \dots, N\} \end{aligned} \quad (19)$$

where $\theta_k(s) = \tan^{-1}(\beta'_k(s) / \alpha'_k(s))$ is the angle between x - and t -axes and prime denotes differentiation with respect to the argument.

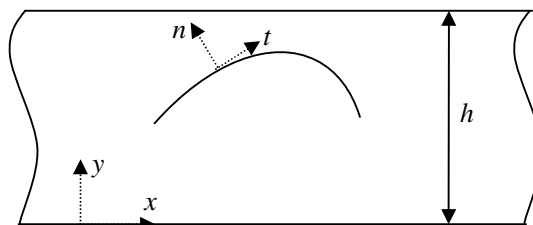


Fig. 2. An arbitrary crack in a strip with orthogonal coordinate system (n, t)

A crack may be constructed by continuous distribution of the dislocations. Suppose dislocation with unknown densities, $B_{wz}(t), B_{\phi z}(t)$, are distributed on the infinitesimal segment $\sqrt{[\alpha'_j(t)]^2 + [\beta'_j(t)]^2} dt$ at the surface of j th crack. Therefore the antiplane traction and electric potential on the surface of the k th crack due to the presence of above-mentioned distribution of the dislocations on all N cracks yields

$$\begin{aligned}\sigma_{nz}(\alpha_k(s), \beta_k(s)) &= \sum_{j=1}^N \int_{-1}^1 \left[\sigma_{yz}^{(1)}(\alpha_k, \beta_k, \alpha_j, \beta_j) \cos(\theta_k) - \sigma_{xz}^{(1)}(\alpha_k, \beta_k, \alpha_j, \beta_j) \sin(\theta_k) \right] dl \\ &\quad 0 \leq \beta_k \leq \beta_j \\ \sigma_{nz}(\alpha_k(s), \beta_k(s)) &= \sum_{j=1}^N \int_{-1}^1 \left[\sigma_{yz}^{(2)}(\alpha_k, \beta_k, \alpha_j, \beta_j) \cos(\theta_k) - \sigma_{xz}^{(2)}(\alpha_k, \beta_k, \alpha_j, \beta_j) \sin(\theta_k) \right] dl \\ &\quad \beta_j \leq \beta_k \leq h \\ D_n(\alpha_k(s), \beta_k(s)) &= \sum_{j=1}^N \int_{-1}^1 \left[D_y^{(1)}(\alpha_k, \beta_k, \alpha_j, \beta_j) \cos(\theta_k) - D_x^{(1)}(\alpha_k, \beta_k, \alpha_j, \beta_j) \sin(\theta_k) \right] dl \\ &\quad 0 \leq \beta_k \leq \beta_j \\ D_n(\alpha_k(s), \beta_k(s)) &= \sum_{j=1}^N \int_{-1}^1 \left[D_y^{(2)}(\alpha_k, \beta_k, \alpha_j, \beta_j) \cos(\theta_k) - D_x^{(2)}(\alpha_k, \beta_k, \alpha_j, \beta_j) \sin(\theta_k) \right] dl \\ &\quad \beta_j \leq \beta_k \leq h \\ &\quad -1 \leq s \leq 1, \quad k \in \{1, 2, \dots, N\}\end{aligned}$$

The functions $\sigma_{mz}^l(\alpha_k, \beta_k, \alpha_j, \beta_j), D_m^l(\alpha_k, \beta_k, \alpha_j, \beta_j), l=1,2, m=x,y$ may be implied by applying (18) to (A-1) and $dl = \sqrt{[\alpha_j'(t)]^2 + [\beta_j'(t)]^2} dt$. The system of integral equations (20) can be written in the following form which will be utilized in numerical procedure.

$$\begin{aligned}\sigma_{nz}(\alpha_k(s), \beta_k(s)) &= \sum_{j=1}^N \int_{-1}^1 \left[K_{ij}^{11}(s,t) \sqrt{[\alpha_j'(t)]^2 + [\beta_j'(t)]^2} B_{wj}(t) + K_{ij}^{12}(s,t) \sqrt{[\alpha_j'(t)]^2 + [\beta_j'(t)]^2} B_{\phi j}(t) \right] dt \\ D_n(\alpha_k(s), \beta_k(s)) &= \sum_{j=1}^N \int_{-1}^1 \left[K_{ij}^{21}(s,t) \sqrt{[\alpha_j'(t)]^2 + [\beta_j'(t)]^2} B_{wj}(t) + K_{ij}^{22}(s,t) \sqrt{[\alpha_j'(t)]^2 + [\beta_j'(t)]^2} B_{\phi j}(t) \right] dt \\ &\quad -1 \leq s \leq 1, \quad k \in \{1,2,\dots,N\}\end{aligned}\quad (21)$$

For brevity the functions $K_{ij}^{11}(s,t)$ are not given and can be achieved by applying equations (A-1) to (20). By virtue of the Buckner's principle, the opposite sign loading in the locations of cracks in the strip in the absence of cracks should be substituted in equations (19), while σ_{nz} and D_n in (19) are the traction and electric potential on a crack surface which is the left-hand side of equations (21). Employing the definition of dislocation density function, the equations for the crack opening displacement and electric potential across the j th crack become (Fotuhi and Fariborz, 2006)

$$\begin{aligned}w_j^-(s) - w_j^+(s) &= \int_{-1}^s \sqrt{[\alpha_j'(t)]^2 + [\beta_j'(t)]^2} B_{wj}(t) dt \\ \phi_j^-(s) - \phi_j^+(s) &= \int_{-1}^s \sqrt{[\alpha_j'(t)]^2 + [\beta_j'(t)]^2} B_{\phi j}(t) dt\end{aligned}\quad (22)$$

The displacement and electric potential field is single-valued out of crack surfaces. Thus, the dislocation density for an embedded crack is subjected to the following closure requirement

$$\int_{-1}^1 \sqrt{[\alpha_j'(t)]^2 + [\beta_j'(t)]^2} B_{kj}(t) dt = 0 \quad k \in \{w, \phi\} \quad (23)$$

which is adopted for each crack j , separately. To obtain the dislocation density for embedded cracks, the integral equations (21) and (23) are to be solved simultaneously whereas for edge

cracks equations (23) are not applicable. Due to the nature of singularity at an embedded crack tip, the following substitution is applied to the system of equations.

$$B_{kj}(t) = \frac{g_{kj}(t)}{\sqrt{1-t^2}}, \quad -1 \leq t \leq 1, \quad k \in \{w, \phi\} \quad (24)$$

The parameters (g_{kj}) are obtained via solution of the system of equations. The stress intensity factor may be written in terms of crack opening (Erdogan, 1985). Similarly, this equation may be extended for FGP materials. Thus the stress and electric intensity factors for i th crack in terms of crack opening displacement and electrical potential take the form

$$\begin{aligned} (K_{III})_{Li} &= \frac{\sqrt{2}}{4} c_{44} (y_{Lj}) \lim_{r_{Li} \rightarrow 0} \frac{w_i^-(s) - w_i^+(s)}{\sqrt{r_{Li}}} + \frac{\sqrt{2}}{4} e_{15} (y_{Lj}) \lim_{r_{Li} \rightarrow 0} \frac{\phi_i^-(s) - \phi_i^+(s)}{\sqrt{r_{Li}}} \\ (K_{III})_{Ri} &= \frac{\sqrt{2}}{4} c_{44} (y_{Rj}) \lim_{r_{Ri} \rightarrow 0} \frac{w_i^-(s) - w_i^+(s)}{\sqrt{r_{Ri}}} + \frac{\sqrt{2}}{4} e_{15} (y_{Rj}) \lim_{r_{Ri} \rightarrow 0} \frac{\phi_i^-(s) - \phi_i^+(s)}{\sqrt{r_{Ri}}} \\ (K_D)_{Li} &= \frac{\sqrt{2}}{4} e_{15} (y_{Lj}) \lim_{r_{Li} \rightarrow 0} \frac{w_i^-(s) - w_i^+(s)}{\sqrt{r_{Li}}} - \frac{\sqrt{2}}{4} d_{11} (y_{Lj}) \lim_{r_{Li} \rightarrow 0} \frac{\phi_i^-(s) - \phi_i^+(s)}{\sqrt{r_{Li}}} \\ (K_D)_{Ri} &= \frac{\sqrt{2}}{4} e_{15} (y_{Rj}) \lim_{r_{Ri} \rightarrow 0} \frac{w_i^-(s) - w_i^+(s)}{\sqrt{r_{Ri}}} - \frac{\sqrt{2}}{4} d_{11} (y_{Rj}) \lim_{r_{Ri} \rightarrow 0} \frac{\phi_i^-(s) - \phi_i^+(s)}{\sqrt{r_{Ri}}} \end{aligned} \quad (25)$$

where the left and right crack tips are depicted by the subscripts L and R, respectively, and

$$r_{Li} = \left[(\alpha_i(s) - \alpha_i(-1))^2 + (\beta_i(s) - \beta_i(-1))^2 \right]^{\frac{1}{2}}, \quad r_{Ri} = \left[(\alpha_i(s) - \alpha_i(1))^2 + (\beta_i(s) - \beta_i(1))^2 \right]^{\frac{1}{2}} \quad (26)$$

Utilizing equations (22, 24, 25) and employing L'Hopital's rule yields the field intensity factors for embedded cracks

$$\begin{aligned}
 (K_{III}^{\sigma})_{L_j} &= \frac{c_{44}(y_{L_j})}{2} \left[[\alpha'_j(-1)]^2 + [\beta'_j(-1)]^2 \right]^{\frac{1}{4}} g_{wj}(-1) + \frac{e_{15}(y_{L_j})}{2} \left[[\alpha'_j(-1)]^2 + [\beta'_j(-1)]^2 \right]^{\frac{1}{4}} g_{\phi_j}(-1) \\
 (K_{III}^{\sigma})_{R_j} &= -\frac{c_{44}(y_{R_j})}{2} \left[[\alpha'_j(1)]^2 + [\beta'_j(1)]^2 \right]^{\frac{1}{4}} g_{wj}(1) - \frac{e_{15}(y_{R_j})}{2} \left[[\alpha'_j(1)]^2 + [\beta'_j(1)]^2 \right]^{\frac{1}{4}} g_{\phi_j}(1), \\
 (K_{III}^D)_{L_j} &= \frac{e_{15}(y_{L_j})}{2} \left[[\alpha'_j(-1)]^2 + [\beta'_j(-1)]^2 \right]^{\frac{1}{4}} g_{wj}(-1) - \frac{d_{11}(y_{L_j})}{2} \left[[\alpha'_j(-1)]^2 + [\beta'_j(-1)]^2 \right]^{\frac{1}{4}} g_{\phi_j}(-1) \\
 (K_{III}^D)_{R_j} &= -\frac{e_{15}(y_{R_j})}{2} \left[[\alpha'_j(1)]^2 + [\beta'_j(1)]^2 \right]^{\frac{1}{4}} g_{wj}(1) + \frac{d_{11}(y_{R_j})}{2} \left[[\alpha'_j(1)]^2 + [\beta'_j(1)]^2 \right]^{\frac{1}{4}} g_{\phi_j}(1),
 \end{aligned} \tag{27}$$

Analogously, for an edge crack with embedded tip at $t = -1$, the dislocation density is

$$B_{kj}(t) = \frac{g_{kj}(t)}{\sqrt{1+t}}, \quad -1 \leq t \leq 1, \quad k \in \{1, 2\} \tag{28}$$

For an edge crack with embedded crack tip at $t = -1$, a similar procedure results in

$$\begin{aligned}
 (K_{III}^{\sigma})_{L_j} &= c_{44}(y_{L_j}) \left[[\alpha'_j(-1)]^2 + [\beta'_j(-1)]^2 \right]^{\frac{1}{4}} g_{wj}(-1) + e_{15}(y_{L_j}) \left[[\alpha'_j(-1)]^2 + [\beta'_j(-1)]^2 \right]^{\frac{1}{4}} g_{\phi_j}(-1) \\
 (K_{III}^D)_{L_j} &= e_{15}(y_{L_j}) \left[[\alpha'_j(-1)]^2 + [\beta'_j(-1)]^2 \right]^{\frac{1}{4}} g_{wj}(-1) - d_{11}(y_{L_j}) \left[[\alpha'_j(-1)]^2 + [\beta'_j(-1)]^2 \right]^{\frac{1}{4}} g_{\phi_j}(-1)
 \end{aligned} \tag{29}$$

Having applied the equations (24, 28) to the integral equations (21) and (23), and discretizing the domain, $-1 \leq t \leq 1$ into $M+1$ segments, a system of $2N \times M$ algebraic equations is obtained which can be solved by the procedure developed by Faal et al. (2006). The resulting system of equations is

$$\begin{bmatrix} C_{11} & C_{12} & \cdots & C_{1N} \\ C_{21} & C_{22} & \cdots & C_{2N} \\ \vdots & \vdots & \ddots & \vdots \\ C_{N1} & C_{N2} & \cdots & C_{NN} \end{bmatrix} \begin{bmatrix} G_1(t_k) \\ G_2(t_k) \\ \vdots \\ G_N(t_k) \end{bmatrix} = \begin{bmatrix} q_1(s_r) \\ q_2(s_r) \\ \vdots \\ q_N(s_r) \end{bmatrix} \tag{30}$$

while the components are mentioned in Appendix C and the collocation points are

$$\begin{aligned} s_r &= \cos\left(\frac{\pi r}{M}\right), \quad r = 1, 2, \dots, M-1 \\ t_p &= \cos\left(\frac{\pi(2p-1)}{2M}\right), \quad p = 1, 2, \dots, M \end{aligned} \quad (31)$$

The solution for g_{kj} are obtained from the above mentioned system of equations and are plugged into equations (27, 29) thereby obtaining the field intensity factors.

4. Numerical examples and discussion

The accuracy of the results will be analyzed by comparison with those available in the literature. Furthermore, the applicability of the DDT will be studied for some other configurations of cracks.

As the first example (Fig. 3a), an functionally graded (FG) strip is considered, having a straight crack under constant loading $\sigma_{yz}=\sigma_0$ on the edges and $\sigma_{xz}=\sigma_0$ as far field traction for $|x|\rightarrow\infty$. The crack may have angle θ with the edge of the strip. For an FG strip we should apply $e_{15}=0$. The crack LR with length $2L/h=0.5$ is rotating around its center which is fixed on the center-line of strip. The variation of dimensionless stress intensity factors (divided by $K_0^s = \sigma_0\sqrt{L}$) versus the angle of rotation for isotropic strip, i.e., $\kappa L=0$ and FG strip with $\kappa L=0.5$ are depicted in Fig. 3b. The results are coincident with those reported in (Fotuhi and Fariborz, 2006). Furthermore, it is possible to verify the stress components for the case of functionally graded materials with no piezoelectric effect. By applying $e_{15}=0$ and $d_{11}=0$, the stress components in equations (16) will be simplified for functionally graded materials which are identical to the equations (13) in the article of Fotuhi and Fariborz (2006).

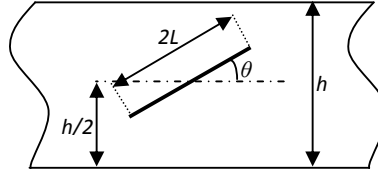


Fig. 3a. A rotating crack in an FG strip

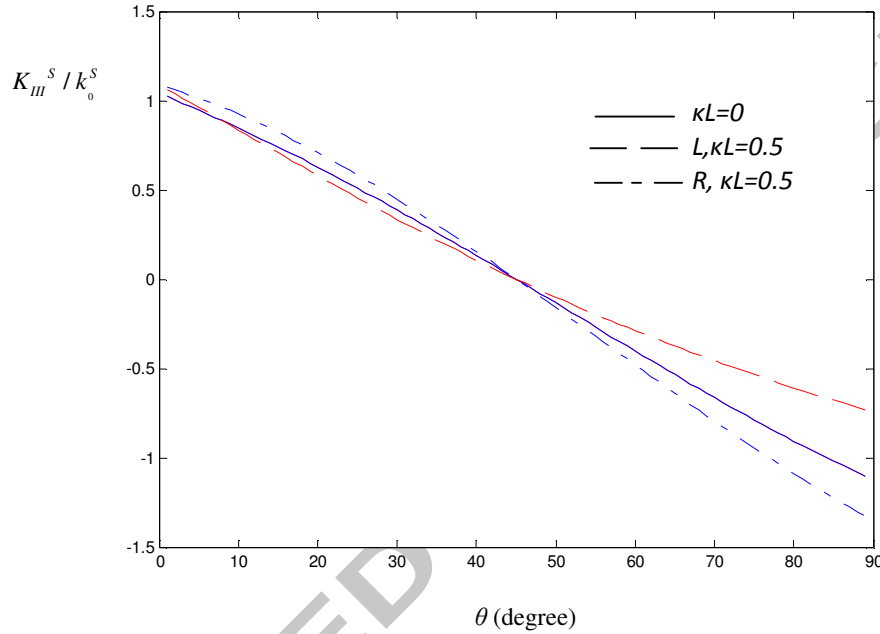


Fig. 3b. Dimensionless stress intensity factors for a rotating crack in an FG strip

In the following examples, the piezoelectric material is assumed to be the commercially available piezoelectric PZT-4. The material constants are $c_{44}=2.56 \times 10^{10}$ N/m², $e_{15}=12.7$ C/m², $d_{11}=64.6 \times 10^{-10}$ C/Vm², respectively. The stress intensity factor is normalized by $K_0^S = \sigma_0 \sqrt{L}$ and the electric intensity factor is normalized by $K_0^D = \sigma_0 e_{15} \sqrt{L} / c_{44}$. Additionally the electromechanical coupling factor is defined by $\lambda = D_0 e_{15} / (\sigma_0 d_{11})$ to combine the shear σ_0 and electrical loading D_0 .

The second example is a strip weakened by a horizontal crack with length $2L/h=0.5$, under constant loading $\sigma_{yz}=\sigma_0$, $D_y=D_0$ on the edges while $\lambda=0.5$ (Fig. 4a). Here the effect of crack

location (d) and gradient parameter is under consideration and the variation of normalized stress intensity factors versus d/L for $\kappa L=0,1,2$ is depicted in Fig. 4b and 4c. The result depicts the effect of the edge and gradient parameter on the field intensity factors. By increasing the gradient parameter, the field factors increase. It is observed that the gradient parameter is less effective near lower boundary.

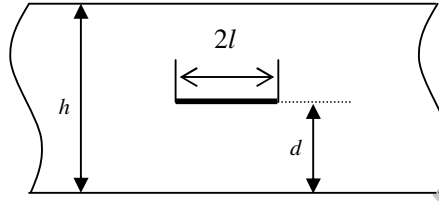


Fig. 4a. A straight crack in an FGP strip

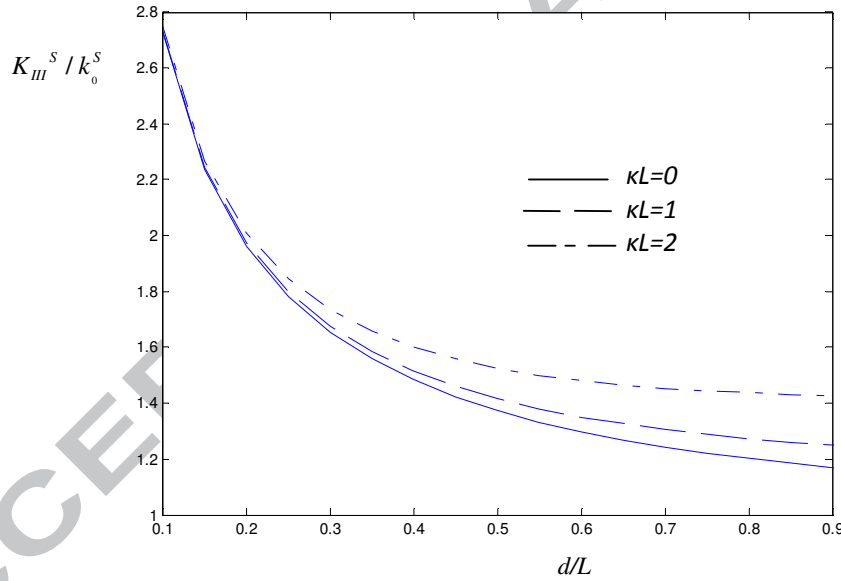


Fig. 4b. Dimensionless stress intensity factors for a crack in an FGP strip

By changing the applied mechanical loading in the above example, it is observed that the electric intensity factor is independent of the mechanical loading which has been reported for a horizontal crack in FGP strip by Ma et al. (2005b) and Pak and Goloubeva (1996). It is

found that the stress and electric field intensity factors demonstrate similar behaviors with respect to the crack configuration (Pak and Goloubeva, 1996).

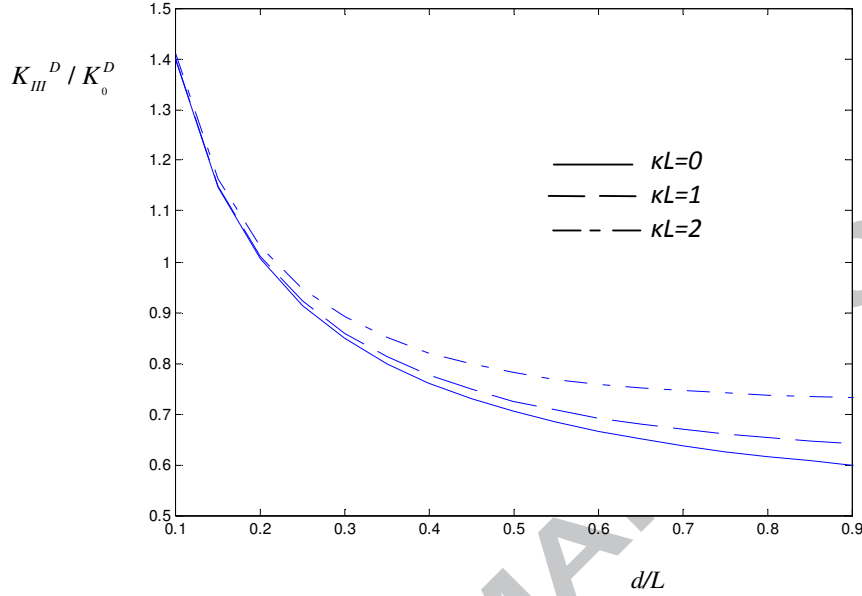


Fig. 4c. Dimensionless electric intensity factors for a crack in an FGP strip

In the next example, the variation of normalized electric intensity factor for a rotating crack in homogeneous and nonhomogeneous ($\kappa L = 2$) strip is studied. The cracked strip is assumed to be under constant loading $\sigma_{yz} = \sigma_{xz} = \sigma_0$, $D_y = D_0$ on the edges with $\lambda = 1$. Similar to the first example (Fig. 3a), the crack LR with length $2L/h = 0.5$ may have the angle θ with the edge and is rotating around its center which is fixed on the center-line of strip. The results are presented in Fig. 5a, 5b. For vertical crack, the electric intensity factor is vanishing due to the electric loading on the edge. There is a peak for electric intensity factor at right crack tip when $\theta = 20^\circ$ which is the interaction of loading, gradation parameter and edge effect. On the other hand, the left crack tip will be reduced by increasing the angle. The reason is the nonhomogeneity of the strip in vertical direction. As FG strip, the stress intensity factors for FGP strip are coincident in $\theta = 45^\circ$. Since there is no traction stress on the crack surface for

$\theta=45^\circ$, the stress intensity factors are zero. Also due to the symmetry for isotropic strip, the stress intensity factors for crack tips are identical.

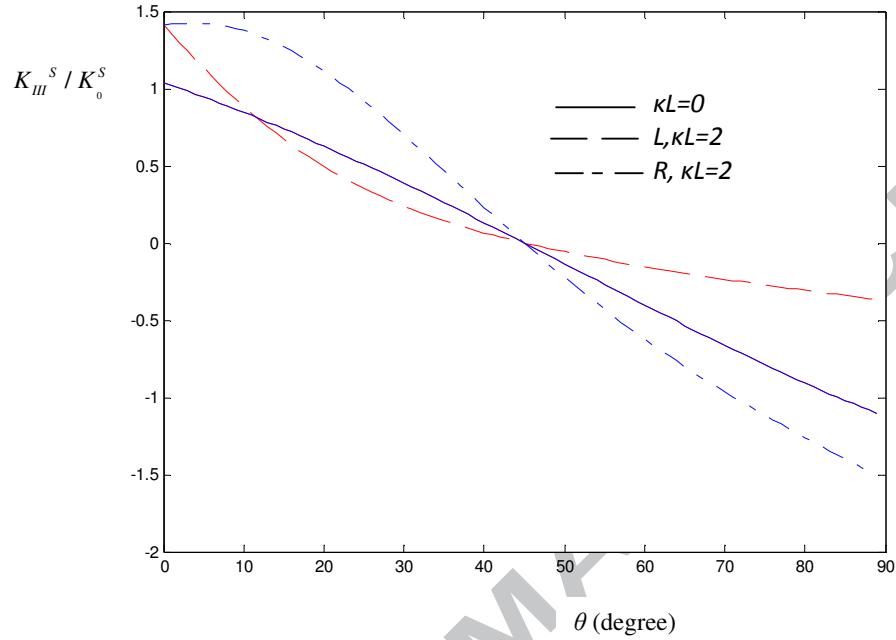


Fig. 5a. Dimensionless stress intensity factors for a rotating crack in an FGP strip

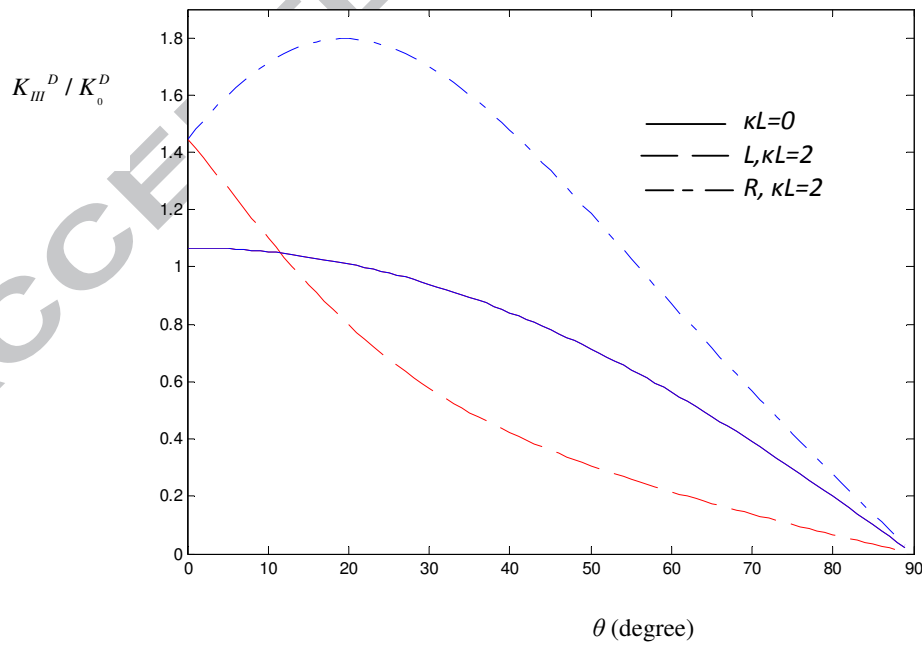


Fig. 5b. Dimensionless electric intensity factors for a rotating crack in an FGP strip

In the following example, the interaction of a fixed and a rotating crack is under consideration in a homogeneous piezoelectric strip. The strip is under constant loading $D_y=D_0$ on the edges, and the gradation parameter is assumed to be $\kappa L=1$. Two equal-length straight cracks are situated on the center-line of the strip (Fig. 6a). Crack L_1R_1 is fixed while L_2R_2 is rotating around its center. Fig. 6b depicts the normalized electric intensity factor for the FGP strip. For $\theta=45^\circ$, the electric intensity factor is identical for crack tip (R_1, L_2) and also (L_1, R_2) . Also for $\theta=45^\circ$, the traction vanishes on the second crack and the electric intensity factor is zero. The interaction of two cracks may be observed in Fig. 6b which is the capability of DDT. This example depicts the capability of the current technique in the solution of piezoelectric strip with interacting cracks.

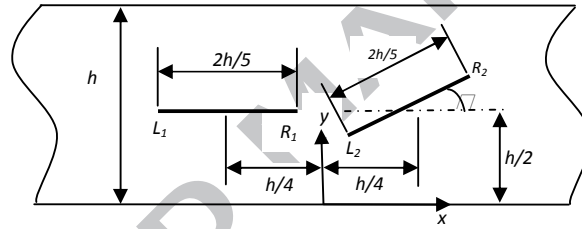


Fig. 6a. A fixed and a rotating crack in an FGP strip

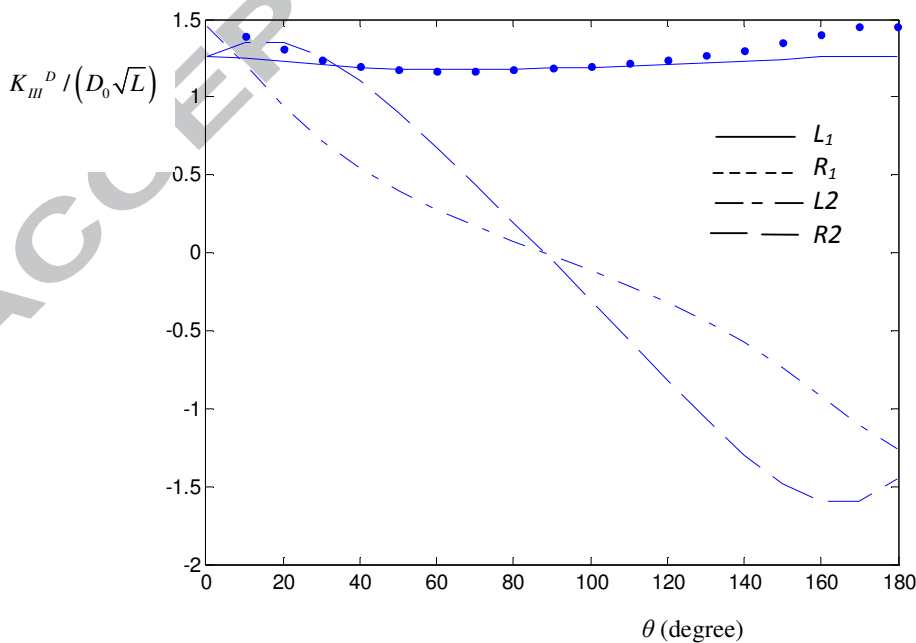


Fig. 6b. Dimensionless electric intensity factors for interaction of cracks in an FGP strip

In the final example, the interaction of two curved cracks in a FGP strip is analyzed. The curved cracks are assumed to be portions of the circumference of an ellipse with the following parametric representations (Fig. 7a):

$$\begin{aligned}\alpha_i(t) &= x_c + a(-1)^i \cos\left[\frac{1}{2}(1-(-1)^i t)\psi\right] \\ \beta_i(t) &= y_c + b \sin\left[\frac{1}{2}(1-(-1)^i t)\psi\right] \quad -1 \leq t \leq 1, \quad i=1,2\end{aligned}$$

while $\psi = \tan^{-1}(a/b \cot(\theta))$ and $(x_c, y_c) = (0, 0.3h)$ is the coordinates of the center of the ellipse. The lengths of major and minor semiaxes of the ellipse are $a/h=0.7$ and $b/h=0.5$, respectively. The nonhomogeneous ($\kappa L=1$) strip is considered to be under constant loading $\sigma_{yz} = \sigma_{xz} = \sigma_0$, $D_y = D_x = D_0$ on the edges with $\lambda=2$. The problem is symmetric with respect to the y -axis. The variations of dimensionless field intensity factors against angle θ for the crack $L_1 R_1$ are shown in Fig. 7b, 7c. At the left tip of crack $L_1 R_1$, the magnitude of electric intensity factor is higher. In this case, the peak points for intensity factors occurs at the angle of about $\theta=50^\circ$. At the right tip of crack $L_1 R_1$, the field intensity factors vanish for the curved cracks with $\theta=45^\circ$. The magnitude of the electric intensity factor is higher than the stress intensity factor at the right tip. When θ approaches to zero, due to the interaction of two cracks, the intensity factors are increasing rapidly.

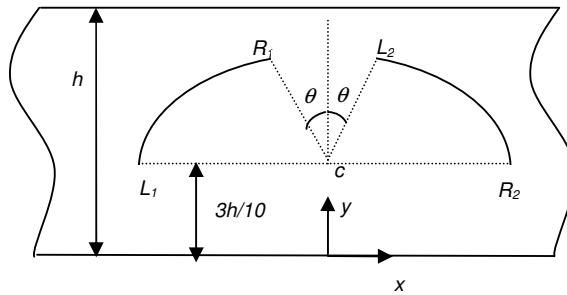


Fig. 7a. Two curved cracks in an FGP strip

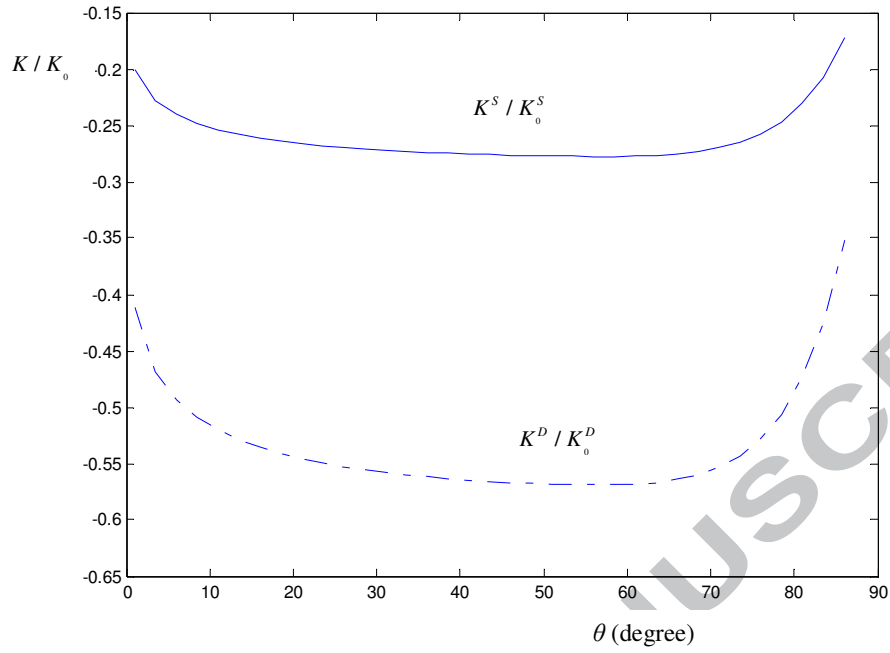


Fig. 7b. Dimensionless field intensity factors at the left tip (L_I) for interaction of two curved cracks in an FGP strip

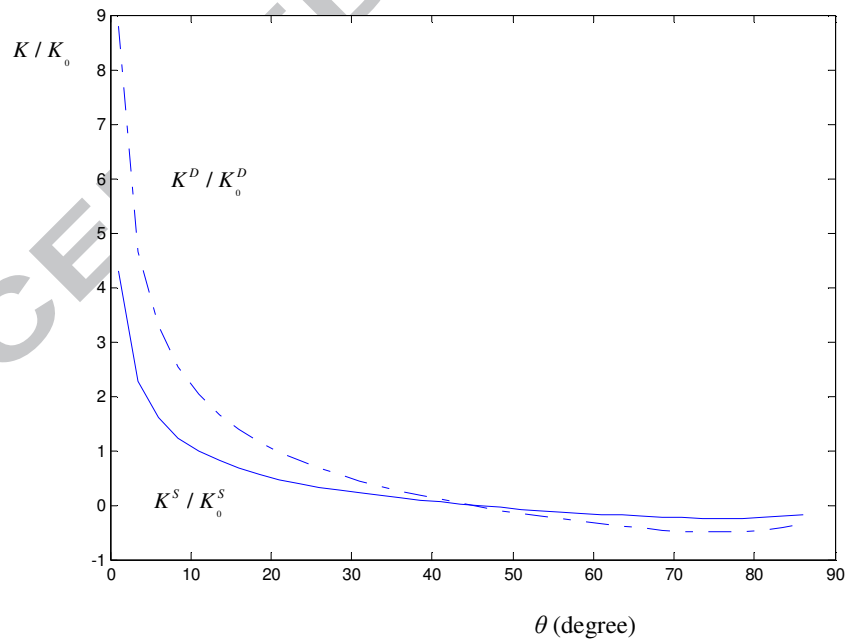


Fig. 7c. Dimensionless field intensity factors at the right tip (R_I) for interaction of two curved cracks in an FGP strip

5. Conclusions

The antiplane analysis of a functionally graded piezoelectric strip containing one or two arbitrary cracks has been carried out utilizing the distributed dislocation technique (DDT). The widely used impermeable condition is assumed in the crack model. The dislocation solution for the strip is attained which contain Cauchy singularity at the location of a dislocation for the stress and electric displacement components. Additionally, the line of dislocation is arbitrary and does not affect the field equation of a dislocation in the domain.

According to the capability of the DDT, the analysis of various arrangements of embedded and edge cracks can be tackled and the stress and electric intensity factors may be evaluated. Several examples are presented and the influence of gradation and loading besides the interaction of multiple straight and curved cracks are studied. It is found that the stress and electric field intensity factors demonstrate similar behavior with respect to the crack configuration.

References

- Abramowitz M, Stegun IA (1964) Handbook of mathematical functions. National Bureau of Standards, Appl Math Series.
- Asadi, E., 2011, Analysis of multiple axisymmetric annular cracks in a piezoelectric medium, Eur. J. Mech. A-Solid 30, 844–853.
- Bleustein, J. L., 1968, A new surface wave in piezoelectric materials. Appl. Phys. Lett. 13, 412–413.

- Chen, J., Liu, Z., Zou, Z., 2003, The central crack problem for a functionally graded piezoelectric strip, *Int. J. Fract.* 121, 81–94.
- Chen, J., Soh, A.K., Liu, J., Liu, Z.X., 2004, Transient anti-plane crack problem of a functionally graded piezoelectric strip bonded to elastic layers, *Acta Mech.* 169, 87–100.
- Chen, J., Liu, Z., 2005, On the dynamic behavior of a functionally graded piezoelectric strip with periodic cracks vertical to the boundary, *Int. J. Solids Struct.* 42, 3133–3146.
- Erdogan, F., 1985, The crack problem for bonded nonhomogeneous materials under antiplane shear loading, *ASME J. Appl. Mech.* 52, 823–828.
- Erdogan, F., Ozturk, M., 1992, Diffusion problems in bonded nonhomogeneous materials with an interface cut, *Int. J. Eng. Sci.* 30, 1507–1523.
- Faal, R.T., Fariborz, S.J., Daghighi, H.R., 2006, Antiplane deformation of orthotropic strips with multiple defects, *J. Mech. Mater. Struct.* 1, 1097–1114.
- Fotuhi, A.R., Fariborz, S.J., 2006, Anti-plane analysis of a functionally graded strip with multiple cracks, *Int. J. Solids Struct.* 43, 1239–1252.
- Han, X., Wang, T., 1999, Interacting multiple cracks in piezoelectric materials, *Int. J. Solids Struct.* 36, 4183–4202.
- Korsunsky, A.M., Hills, D.A., 1996, The solution of crack problems by using distributed strain nuclei, *P I Mech. Eng. C-J Mec.* 210, 23–31.
- Kuna, M., 2010, Fracture mechanics of piezoelectric materials – Where are we right now?, *Eng. Fract. Mech.* 77, 309–326.

Ma, L., Wu, L., Zhou, Z., Guo, L., 2004, L. Shi, Scattering of harmonic anti-plane shear waves by two collinear cracks in functionally graded piezoelectric materials, *Eur. J. Mech. A-Solid* 23, 633–643.

Ma L., Wu, L., Zhou, Z., Guo, L., 2005a, Scattering of the harmonic anti-plane shear waves by a crack in functionally graded piezoelectric materials, *Comp. Struct.* 69, 436–441.

Ma, L., Wu, L., Zhou, Z., Guo, L., 2005b, Fracture analysis of a functionally graded piezoelectric strip, *Comp. Struct.* 69, 294–300.

Mousavi, S.M., Fariborz, S.J., 2012, Anti-plane elastodynamic analysis of cracked graded orthotropic layers with viscous damping, *Appl. Math. Model.* 36, 1626–1638.

Narita, F., Shindo, Y., 1999, Scattering of antiplane shear waves by a finite crack in piezoelectric laminates, *Acta Mech.* 134, 27–43.

Pak, Y.E., Golubeva, E., 1996, Electroelastic properties of cracked piezoelectric materials under longitudinal shear, *Mech. Mater.* 24, 287–303.

Parton, V.Z. , Mikhailov, G.K. , 1990, *Electromagnetoelasticity*, Newyork, Hemisphere.

Sosa, H. , 1992, On the fracture mechanics of piezoelectric solids, *Int. J. Solids Struct.* 29, 2613–2622.

Wang, X.Y., Yu, S.W., 2000, Transient response of a crack in a piezoelectric strip objected to the mechanical and electrical impacts: mode III problem, *Int. J. Solids Struct.* 37, 5795–5808.

Wang, X.D., Jiang, L.Y., 2002, Nonlinear behaviour of interacting dielectric cracks in piezoelectric materials, *Int. J. Solids Struct.* 39, 585–600.

Appendix A

The following functions are used in the field components.

$$P_1(\gamma_1, \gamma_2) = \int_{-\infty}^{+\infty} \frac{[\beta \cosh(\beta \gamma_1) + \kappa \sinh(\beta \gamma_1)] \sinh(\beta \gamma_2)}{s \beta \sinh(\beta h)} \exp(is(x - \eta)) ds \quad (A-1)$$

$$P_2(\gamma_1, \gamma_2) = \int_{-\infty}^{+\infty} \frac{[\beta \cosh(\beta \gamma_1) + \kappa \sinh(\beta \gamma_1)] \sinh(\beta \gamma_2)}{\beta \sinh(\beta h)} \exp(is(x - \eta)) ds \quad (A-2)$$

$$P_3(\gamma_1, \gamma_2) = \int_{-\infty}^{+\infty} \frac{\sinh(\beta \gamma_1) \sinh(\beta \gamma_2)}{\beta \sinh(\beta h)} s \exp(is(x - \eta)) ds \quad (A-3)$$

Appendix B:

The field components with separated singular terms are:

$$\sigma_{xz} = \frac{(b_{wz} c_{44}^0 + b_{\phi z} e_{15}^0) e^{\kappa(y+\zeta)}}{\pi} \int_0^{+\infty} \left[\frac{[\beta \cosh(\beta y) + \kappa \sinh(\beta y)] \sinh(\beta(h - \zeta))}{\beta \sinh(\beta h)} - \frac{1}{2} e^{s(y-\zeta)} \right] \cos(s(x - \eta)) ds$$

$$- \frac{(b_{\phi z} e_{15}^0 + b_{wz} c_{44}^0) e^{\kappa(y+\zeta)}}{2\pi} \frac{(y - \zeta)}{(x - \eta)^2 + (y - \zeta)^2} \quad 0 \leq y \leq \zeta$$

$$\sigma_{xz} = - \frac{(b_{wz} c_{44}^0 + b_{\phi z} e_{15}^0) e^{\kappa(y+\zeta)}}{\pi}$$

$$\times \int_0^{+\infty} \left[\frac{[\beta \cosh(\beta(y - h)) + \kappa \sinh(\beta(y - h))] \sinh(\beta \zeta)}{\beta \sinh(\beta h)} - \frac{1}{2} e^{-s(y-\zeta)} \right] \cos(s(x - \eta)) ds$$

$$- \frac{(b_{\phi z} e_{15}^0 + b_{wz} c_{44}^0) e^{\kappa(y+\zeta)}}{2\pi} \frac{(y - \zeta)}{(x - \eta)^2 + (y - \zeta)^2} \quad \zeta \leq y \leq h$$

$$\begin{aligned}\sigma_{yz} &= \frac{(b_{wz}c_{44}^0 + b_{\phi z}e_{15}^0)e^{\kappa(y+\zeta)}}{\pi} \int_0^{+\infty} \left[s \frac{\sinh(\beta y) \sinh(\beta(h-\zeta))}{\beta \sinh(\beta h)} - \frac{1}{2} e^{s(y-\zeta)} \right] \sin(s(x-\eta)) ds \\ &+ \frac{(c_{44}^0 b_{wz} + b_{\phi z} e_{15}^0) e^{\kappa(y+\zeta)}}{2\pi} \frac{(x-\eta)}{(x-\eta)^2 + (y-\zeta)^2} \quad 0 \leq y \leq \zeta\end{aligned}$$

$$\begin{aligned}\sigma_{yz} &= -\frac{(b_{wz}c_{44}^0 + b_{\phi z}e_{15}^0)e^{\kappa(y+\zeta)}}{\pi} \int_0^{+\infty} \left[s \frac{\sinh(\beta(y-h)) \sinh(\beta\zeta)}{\beta \sinh(\beta h)} + \frac{1}{2} e^{-s(y-\zeta)} \right] \sin(s(x-\eta)) ds \\ &+ \frac{(b_{\phi z}e_{15}^0 + c_{44}^0 b_{wz}) e^{\kappa(y+\zeta)}}{2\pi} \frac{(x-\eta)}{(x-\eta)^2 + (y-\zeta)^2} \quad \zeta \leq y \leq h\end{aligned}$$

$$\begin{aligned}D_x &= \frac{(b_{wz}e_{15}^0 - b_{\phi z}d_{11}^0)e^{\kappa(y+\zeta)}}{\pi} \\ &\times \int_0^{+\infty} \left[\frac{[\beta \cosh(\beta y) + \kappa \sinh(\beta y)] \sinh(\beta(h-\zeta))}{\beta \sinh(\beta h)} - \frac{1}{2} e^{s(y-\zeta)} \right] \cos(s(x-\eta)) ds \\ &- \frac{(b_{wz}e_{15}^0 - b_{\phi z}d_{11}^0)e^{\kappa(y+\zeta)}}{2\pi} \frac{(y-\zeta)}{(x-\eta)^2 + (y-\zeta)^2} \quad 0 \leq y \leq \zeta\end{aligned}$$

$$\begin{aligned}D_x &= -\frac{(b_{wz}e_{15}^0 - b_{\phi z}d_{11}^0)e^{\kappa(y+\zeta)}}{\pi} \\ &\times \int_0^{+\infty} \left[\frac{[\beta \cosh(\beta(y-h)) + \kappa \sinh(\beta(y-h))] \sinh(\beta\zeta)}{\beta \sinh(\beta h)} - \frac{1}{2} e^{-s(y-\zeta)} \right] \cos(s(x-\eta)) ds \\ &- \frac{(b_{wz}e_{15}^0 - b_{\phi z}d_{11}^0)e^{\kappa(y+\zeta)}}{2\pi} \frac{(y-\zeta)}{(x-\eta)^2 + (y-\zeta)^2} \quad \zeta \leq y \leq h\end{aligned}$$

$$\begin{aligned}
 D_y &= \frac{(b_{wz}e_{15}^0 - b_{\phi z}d_{11}^0)e^{\kappa(y+\zeta)}}{\pi} \int_0^{+\infty} \left[\frac{\sinh(\beta y) \sinh(\beta(h-\zeta))}{\beta \sinh(\beta h)} s - \frac{1}{2} e^{s(y-\zeta)} \right] \sin(s(x-\eta)) ds \\
 &\quad + \frac{(b_{wz}e_{15}^0 - b_{\phi z}d_{11}^0)e^{\kappa(y+\zeta)}}{2\pi} \frac{(x-\eta)}{(x-\eta)^2 + (y-\zeta)^2} \quad 0 \leq y \leq \zeta \\
 D_y &= -\frac{(b_{wz}e_{15}^0 - b_{\phi z}d_{11}^0)e^{\kappa(y+\zeta)}}{\pi} \int_0^{+\infty} \left[\frac{\sinh(\beta(y-h)) \sinh(\beta\zeta)}{\beta \sinh(\beta h)} s + \frac{1}{2} e^{-s(y-\zeta)} \right] \sin(s(x-\eta)) ds \\
 &\quad + \frac{(b_{wz}e_{15}^0 - b_{\phi z}d_{11}^0)e^{\kappa(y+\zeta)}}{2\pi} \frac{(x-\eta)}{(x-\eta)^2 + (y-\zeta)^2} \quad \zeta \leq y \leq h
 \end{aligned} \tag{B-1}$$

Appendix C:

The matrix components in equation (30) are:

$$C_{ij} = \begin{bmatrix} \Delta_j(t_1)K_{ij}(s_1, t_1) & \Delta_j(t_2)K_{ij}(s_1, t_2) & \cdots & \Delta_j(t_M)K_{ij}(s_1, t_M) \\ \Delta_j(t_1)K_{ij}(s_2, t_1) & \Delta_j(t_2)K_{ij}(s_2, t_2) & \cdots & \Delta_j(t_M)K_{ij}(s_2, t_M) \\ \vdots & \vdots & \ddots & \vdots \\ \Delta_j(t_1)K_{ij}(s_{M-1}, t_1) & \Delta_j(t_2)K_{ij}(s_{M-1}, t_2) & \cdots & \Delta_j(t_M)K_{ij}(s_{M-1}, t_M) \\ \Delta_j(t_1)B_{ij}(t_1) & \Delta_j(t_2)B_{ij}(t_2) & \cdots & \Delta_j(t_M)B_{ij}(t_M) \end{bmatrix}$$

$$G_j(t_k) = [g_{wj}(t_1) \quad g_{\phi j}(t_1) \quad \cdots \quad g_{wj}(t_M) \quad g_{\phi j}(t_M)]^T, \quad j = 1, \dots, N$$

$$q_j(s_r) = \begin{bmatrix} \sigma_{nz}(x_j(s_1), y_j(s_1)) & D_n(x_j(s_1), y_j(s_1)) & \cdots & \sigma_{nz}(x_j(s_{M-1}), y_j(s_{M-1})) & D_n(x_j(s_{M-1}), y_j(s_{M-1})) \\ 0 & 0 \end{bmatrix}^T, \quad j = 1, \dots, N_1$$

$$q_j(s_r) = \begin{bmatrix} \sigma_{nz}(x_j(s_1), y_j(s_1)) & D_n(x_j(s_1), y_j(s_1)) & \cdots & \sigma_{nz}(x_j(s_{M-1}), y_j(s_{M-1})) & D_n(x_j(s_{M-1}), y_j(s_{M-1})) \\ \sigma_{nz}(x_j(s_M), y_j(s_M)) & D_n(x_j(s_M), y_j(s_M)) \end{bmatrix}^T, \quad j = N_1 + 1, \dots, N$$

$$\Delta_j(t_k) = \frac{\pi}{M} \begin{cases} 1 & j = 1, 2, \dots, N_1 \\ 1 - t_k & j = N_1 + 1, \dots, N \end{cases} \quad k = 1, 2, \dots, M$$

$$B_{ij}(t) = \begin{cases} \delta_{ij} \sqrt{[\alpha'_i(t)]^2 + [\beta'_i(t)]^2} \begin{bmatrix} 1 & 0 \\ 0 & 1 \end{bmatrix}, & i = 1, \dots, N_1 \\ \begin{bmatrix} K_{ij}^{11}(1, t_k) & K_{ij}^{12}(1, t_k) \\ K_{ij}^{21}(1, t_k) & K_{ij}^{22}(1, t_k) \end{bmatrix}, & i = N_1 + 1, \dots, N \end{cases}$$

$$K_{ij}(s_r, t_k) = \begin{bmatrix} K_{ij}^{11}(s_r, t_k) & K_{ij}^{12}(s_r, t_k) \\ K_{ij}^{21}(s_r, t_k) & K_{ij}^{22}(s_r, t_k) \end{bmatrix} \quad (C-1)$$

Figure Caption:

Fig. 1. Schematic view of the FGP strip weakened by a screw dislocation

Fig. 2. An arbitrary crack in a strip with orthogonal coordinate system (n, t)

Fig. 3a. A rotating crack in an FG strip

Fig. 3b. Dimensionless stress intensity factors for a rotating crack in an FG strip

Fig. 4a. A straight crack in an FGP strip

Fig. 4b. Dimensionless stress intensity factors for a crack in an FGP strip

Fig. 4c. Dimensionless electric intensity factors for a crack in an FGP strip

Fig. 5a. Dimensionless stress intensity factors for a rotating crack in an FGP strip

Fig. 5b. Dimensionless electric intensity factors for a rotating crack in an FGP strip

Fig. 6a. A fixed and a rotating crack in an FGP strip

Fig. 6b. Dimensionless electric intensity factors for interaction of crack in an FGP strip

Fig. 7a. Two curved cracks in an FGP strip

Fig. 7b. Dimensionless field intensity factors at the right tip (L_I) for interaction of two curved cracks in an FGP strip

Fig. 7c. Dimensionless field intensity factors at the left tip (R_I) for interaction of two curved cracks in an FGP strip